Published in final edited form as:
J Am Chem Soc. 2012 May 30; 134(21): 8823–8830. doi:10.1021/ja2110703.

RNA encapsidation by SV40-derived nanoparticles follows a rapid two-state mechanism

Stanislav Kler[1,‡], **Roi Asor**[2,‡], **Chenglei Li**[3], **Avi Ginsburg**[2,4], **Daniel Harries**[2,5], **Ariella Oppenheim**[1,*], **Adam Zlotnick**[3,6,*], and **Uri Raviv**[2,*]

[1]Dept. of Hematology, Hebrew University-Hadassah Medical School, Jerusalem, Israel, 91120

[2]Institute of Chemistry, The Hebrew University of Jerusalem, Israel, 91904

[3]Dept. of Molecular and Cellular Biochemistry, Indiana University, Bloomington, IN 47405

[4]The School of Drug research, The Hebrew University of Jerusalem

[5]The Fritz Haber Research center, The Hebrew University of Jerusalem, Israel, 91904

[6]Dept. of Biology, Indiana University, Bloomington, IN 47405

Abstract

Remarkably, uniform virus-like particles self-assemble in a process that appears to follow a rapid kinetic mechanism. The mechanisms by which spherical viruses assemble from hundreds of capsid proteins around nucleic acid, however, are yet unresolved. Using Time-Resolved Small-Angle X-ray Scattering (TR-SAXS) we have been able to directly visualize SV40 VP1 pentamers encapsidating short RNA molecules (500 mers). This assembly process yields $T = 1$ icosahedral particles comprised of 12 pentamers and one RNA molecule. The reaction is nearly 1/3 complete within 35 milliseconds, following a two–state kinetic process with no detectable intermediates. Theoretical analysis of kinetics, using a master equation, shows that the assembly process nucleates at the RNA and continues by a cascade of elongation reactions in which one VP1 pentamer is added at a time, with a rate of approximately 10^9 M^{-1} s^{-1}. The reaction is highly robust and faster than the predicted diffusion limit. The emerging molecular mechanism, which appears to be general to viruses that assemble around nucleic acids, implicates long-ranged electrostatic interactions. The model proposes that the growing nucleo-protein complex acts as an electrostatic antenna that attracts other capsid subunits for the encapsidation process.

Keywords

Time-resolved small-angle X-ray scattering; SV40; virus-like-particles; self-assembly; virus assembly kinetics; virus assembly mechanism

[*]Corresponding Authors: raviv@chem.ch.huji.ac.il, azlotnic@indiana.edu, ariella.oppenheim@mail.huji.ac.il.
[‡]These authors contributed equally.

Author Contributions

The manuscript was written through contributions of all authors./All authors have given approval to the final version of the manuscript.

Supporting Information. Additional supporting figures (Figures S1 to S7) and data analysis are presented in the supporting information. This material is available free of charge via the Internet at http://pubs.acs.org.

INTRODUCTION

Viruses are evolved examples of self-assembled structures that are remarkably sophisticated biological machines. This ability to self-assemble can be harnessed for nano- and bio-technology. Indeed, viral capsids and capsid proteins have been used to assemble structures for guided synthesis of inorganic and organic nanostructures, [1,2] as cages for packaging cargos, [3,4] and as vectors for gene therapy. [5–7] The mechanism of packaging even biologically relevant nucleic acid, however, remained unknown.

An attractive candidate for nanostructural manipulation is the SV40 virus, a small non-enveloped virus belonging to the polyomavirus family. SV40 has a circular double-stranded (ds) DNA genome of 5,243 base pairs compacted by histone octamers to a nucleosomal structure similar to cellular chromatin. [8,9] The 48 nm diameter viral capsid, surrounding the viral minichromosome, is composed of three proteins, VP1, VP2 and VP3. VP1 forms the outer shell while VP2 and VP3 are located internally to VP1 and help bridge it to the chromatin core. Nonetheless, VP1 alone binds DNA with high affinity. [10] VP1 monomers are tightly bound in pentamers ($VP1_5$) through interdigitating β-strands [11] formed immediately following translation. [12] Based on this architecture, SV40 capsids are composed of 72 VP1 pentamers arranged in a $T=7$ lattice. [11,13]

Recombinant $VP1_5$ also assembles cooperatively around circular ds-DNA, to form an icosahedral structure that is similar to wild-type (wt) SV40. [14,15] Such Virus-Like Particles (VLPs) may be used as vectors for gene delivery [5,6] as well as an experimental model system to study assembly reactions. [15] We recently demonstrated a requirement of a nucleic acid for uncatalyzed assembly of purified VP1 under physiological conditions (150 mM NaCl at pH 7.2). We proposed that the nucleic acid served as a nucleation center and/or a scaffold for assembly.

The specific mechanism(s) of how viruses assemble on nucleic acid remains an open question. Experience with assembly of empty capsids [16] suggests that assembly is nucleated and based on weak interactions of multivalent subunits. Weak association allows error correction of mis-incorporated subunits. [17,18] Nucleation prevents a situation where there may be many partial capsids but no complete ones. Nucleation and weak association result in assembly reactions that appear two-state, with few if any intermediates transiently detectable. [19–21]

Many self-assembling virus capsid proteins, including SV40 $VP1_5$, have nucleic acid binding domains that will certainly affect the details of assembly. Observations of assembly reactions that have been given time to equilibrate suggest complex, cooperative behavior. For example, RNA titrations by Hepatitis B Virus capsid protein appear two-state, [22] whereas titrations with Cowpea Chlorotic Mottle Virus capsid protein (which has much weaker self association [23]) appear to be gradual. [24] Describing the pathway of assembly and encapsidation, however, requires rigorous kinetic analysis.

Here we report self-assembly of $T=1$ VLPs from SV40 $VP1_5$, induced by a short RNA polymer. The short ssRNA substrate allowed us to examine the simplest case reaction of dodecahedral assembly, where all pentamers are equivalent. Conversely, assembly with dsDNA is much more complicated: dsDNA leads to a 72 pentamer complex with several different classes of pentamer-pentamer interactions. An additional issue is the work required to bend the dsDNA (with a persistence length of about 50 nm) to fit into an SV40 capsid, with an inner diameter of about 40 nm. To ensure that we could describe progression of the reaction and the presence or absence of intermediates, we followed assembly using high-resolution synchrotron Time-Resolved Small-Angle X-ray Scattering (TR-SAXS). Based on fitting TR-SAXS data to a master equation model of capsid assembly, VLP formation

appeared to be nucleated, where the nucleation step was differentiated from elongation on the basis of kinetics. Assembly rate constants were very fast, leading us to suggest that long-ranged (electrostatic) interactions play a critical role in assembly. The strong negative surface charge, common to most virus capsids, may thus contribute to attracting reactants that facilitate formation of viruses and VLPs, *in vivo* and *in vitro*.

MATERIALS AND METHODS

Protein and RNA for assembly reactions

SV40 VP1 VLPs were produced in Spodoptera frugiperda (Sf9) insect cell and produced as previously described. [15] Pentamers were obtained by dissociating VLPs by dialysis first against 20 mM Tris-Cl, pH 8.9, 50 mM NaCl, 2 mM DTT (dissociation buffer) with 5 mM EDTA and then against dissociation buffer with 2 mM EDTA at 4°C. The dialysate was centrifuged at 20,000g for 30 minutes at 4 °C to sediment aggregated protein. Clarified supernatant was quantified by UV absorbance, using an extinction coefficient of ε_{280} = 32,890 $M^{-1}cm^{-1}$ per VP1 monomer. [25]

We used yeast 75 nucleotides tRNA, 524 nucleotide RNA (500 mer) and 814 nucleotides RNA (800mer) as templates for SV40 VP1 assembly. Yeast 75 nt tRNA was purchased from Ambion. 500 and 800mer RNAs were in vitro transcribed from linearized pETc11-Cp149 using a MegaScript T7 kit (Ambion). Though not fully tested, it is likely that the actual sequence does not make a significant contribution to the details of assembly.

Equilibrated Assembly Reactions

Disassembled VP1 pentamers were mixed with RNA in 2 × assembly buffer (250 mM NaCl, 100 mM MOPS pH 7.2). Samples were examined by electrophoretic mobility shift (EMSA), transmission electron microscopy (TEM), and size exclusion chromatography with absorbance or multi-angle laser light scattering detectors (SEC or SEC-MALLS). For EMSA, samples were electrophoresed through 0.6% agarose gel using a TAE buffer system for 1 hour at 100V constant voltage followed by ethidium bromide staining. [24] Samples for TEM were adsorbed to freshly glow discharged, formvar-carbon coated copper grids (EM sciences) for 3 minutes and stained with 2% uranyl acetate for 30 sec and washed with deionized water. Samples were air dried and visualized on JEOL JEM1010.

Size exclusion chromatography was performed using Bio SEC-5 columns, (7 and 14 ml) with a 500Å pore size (Agilent Technologies) equilibrated with assembly buffer. For abasorbance analysis we used a Shimadzu HPLC with a diode array detector. For SEC-MALLS we used a Shimadzu HPLC pump with tandem DAWN HELEOS II light scattering and Optilab Rex refractive index detectors in tandem (both from Wyatt).

Data collection for SAXS

SAXS measurements were performed at beam-line ID02 in ESRF (Grenoble, France) with 10 keV X-rays from a $Si_{1,1,1}$ monochromator. Silver behenate was used as a standard to determine the sample to detector distance. Data were recorded with a Fast-Readout, Low-Noise (FReLoN) Kodak KAF-4320 CCD-based sensor. [26–28]

To determine the steady-state scattering of $VP1_5$ solution and RNA-containing capsids we used a flow-through setup, composed of a 1.2 mm inner diameter quartz capillary connected to a syringe. RNA-containing capsids were assembled by mixing equal volumes of 10μM of VP1 pentamers with 0.6μM RNA in assembly buffer. After an incubation of 20 min the solution was injected into the flow-through setup and SAXS scans were recorded. The scattering signal from an excess of 1.4 μM $VP1_5$ was subtracted to obtain the signal of the

pure capsid. At equilibrium, most if not all the RNA was consumed, hence, the contribution from unassembled RNA chains to the signal was negligible.

TR-SAXS measurements were recorded by mixing 100 μl of 15 μM $VP1_5$ and 100μl of 1 μM 500 mer RNA, using a BioLogic SFM-400 stopped-flow instrument and a 1.6 mm quartz capillary. Several regimens of data collection were followed to produce the final data set. For four reactions, SAXS was measured for 5 ms starting after delays of 35, 85, 135, or 185 ms and then at intervals of 200 ms, thereby covering the first 2 s of assembly at a sampling density of 50 ms. The fifth reaction was measured for 5 ms starting after a delay of 30 ms followed by 0.995 s intervals, for a total of one minute.

The 2D scattering patterns were radially integrated. [29] The scattering intensity, *I*, was plotted as a function of the magnitude of the momentum transfer vector, *q*, and analyzed using X+ software. [26] A form-factor model of multiple concentric spherical shells with smoothly varying electron density profiles, represented by hyperbolic tangents (eq 1), was fit to the steady-state VLP data, as described [26]

$$\Delta\rho(\mathrm{r})=0.5\left\{\Delta\rho_1+\sum_{\mathrm{i}=1}^{\mathrm{N}-1}\left[(\Delta\rho_{i+1}-\Delta\rho_i)\right]\cdot\tanh\left[\mathrm{s_i}(r-R_i)\right]\right\} \quad (1)$$

$\Delta\rho(r)$ indicates the radial electron density contrast with respect to the solvent (buffer). The index i represents the i-th layer in the sphere, with an outer radius, R_i, an electron density contrast, $\Delta\rho_i$, and connected to the subsequent layer ($i+1$) by a slope s_i. $\Delta\rho_N = 0$ and corresponds to the solvent electron density contrast. The form-factor of the smooth $\Delta\rho(r)$ functions were calculated by discretizing the profiles and transforming them to a sum of Heaviside Step functions that can be analytically solved. [26,30]

RESULTS

Assembly on short RNA

In vitro assembly of SV40 VP1 pentamers ($VP1_5$) on nucleic acid is controlled by protein-protein interaction and the nature of the nucleic acid scaffold. [25] Short, flexible RNA molecules were expected to favor local interactions as they would be too small to interact with the complement of 72 pentamers of the wt SV40 capsid. Binding of VP1 to short RNA was evaluated by electrophoretic mobility shift assay (EMSA), titrating a constant concentration of nucleic acid with increasing amounts of $VP1_5$. Titrations (Figure 1A and Figure S1A) showed a bimodal distribution of free and VP1-bound short RNA for three different RNA substrates, tRNA, and longer 524 nucleotide, and 814 nucleotide substrates. The decrease in the amount of free RNA, measured by ethidium bromide (EtBr) fluorescence in gels, was proportional to the amount of added $VP1_5$, though some smearing was also evident. For all three RNAs, at high $VP1_5$ concentrations, the majority of the EtBr staining material ran as a single slow migrating band.

Size and structure of the capsids

Transmission electron microscopy (TEM) showed that assembly on all three short RNA substrates resulted in capsids of ca. 22 nm (Figures 1B, S1B, and S2), consistent with T=1 particles. The 22 nm particles were first characterized by size exclusion chromatography (SEC) using an HPLC equipped with a diode array absorbance detector to determine the ratio of $VP1_5$ to nucleic acid in the capsids fraction [22] (Figure 1B and Figure S2). After correction for light scattering, the 260/280 absorbance ratio for the particles assembled on the 524 nt RNA was 1.357 ± 0.001, corresponding to one RNA molecule for every 11.5

pentamers, close to the 12 pentamers required for a *T*=1 capsid (the expected 260/280 absorbance ratio for a *T*=1 particle is 1.33). The 260/280 absorbance ratio for the particles assembled on 75 nt RNA was 1.19 (Figure S2), corresponding to two RNA molecules per capsid. To further characterize the 22 nm particles, we focused further experiments on reactions with the 524 nt RNA (hereafter 500 mer RNA). The reaction products appeared to be homogenous by both TEM and SAXS (described later).

In additional experiments, SEC with Multi-Angle Laser Light Scattering (SEC-MALLS) was used to measure the weight-average molecular weight (M_W) and diameter of solute in the capsid fractions. The beginning of the capsid peak included some high molecular weight aggregates and was excluded from the M_W calculation. For fractions eluted from 16.7 minutes to 17.3 minutes (Figure 1C) the M_W and diameter were homogenous. Based on the angular dependence of scattering, the capsid diameter was 22.4±0.4 nm. The weight-average molecular weight was 2.6 ± 0.03 MDa (Figure 1C). This molecular weight is very close to the calculated weight of one 500 mer RNA molecule and twelve 210 kDa VP1 pentamers (150 kDa + 12 × 210 kDa = 2.67 MDa). These results are consistent with assignment of the 22 nm particles as T=1 icosahedra.

SAXS of pentamers and *T*=1 capsids

To describe the X-ray scattering solute to a first approximation, a form-factor of multiple concentric spherical shells with smoothly varying electron density profiles was fit to the data, as previously described. [26]

SAXS of the 500 mer RNA - $VP1_5$ complex (Figure 2) correlates with VLPs that have an outer diameter of 24.5 nm, consistent with TEM and MALLS (Figures 1 and S1). At low q values, the scattering intensity is well fit by a multi-shell spherical model with high electron density at the center, enveloped by a lower density layer, and followed by a high electron density outer layer. This would correspond to a protein shell surrounding an RNA core. The particles appear to be monodisperse as indicated by the adequate fit of the data at the first and third minima. At high resolution (high q values) the simple spherical multi-shell model is insufficient to well fit the data.

TR-SAXS of assembly

TR-SAXS of the reaction of $VP1_5$ and 500 mer, observed over a period of one minute, using a stopped-flow setup, shows a progressive change in the angular dependence of scattering. Overlays of a series of time-resolved measurements (Figure 3A) of the reaction show an isosbestic point at $q \approx 0.25\ nm^{-1}$. Isosbestic points suggest that two states dominate the reaction. Intermediate structures are likely to form but remain at low concentrations, hence negligibly contribute to the scattering signal.

For a two-state reaction, TR-SAXS intensities can be modeled as a sum of the intensities of the reactant and product as follows:

$$I(q,t)=\alpha(t)\times I_{VLP}(q)+\beta(t)\times I_{Pentamers}(q)+\gamma(t)\times I_{RNA}(q) \quad (2)$$

In eq 2, $I_{VLP}(q)$, $I_{Pentamers}(q)$ and $I_{RNA}(q)$ are normalized basis spectra for capsid, $VP1_5$, and RNA, respectively (Figures 2 & S3). The time-dependent coefficients: α, β and γ represent the time-dependent concentrations. As we have observed that VLPs are comprised of one RNA molecule and 12 $VP1_5$, the progression of scattering should be well-described by a single free parameter:

$$I(q,t)=\alpha(t)\times I_{VLP}(q)+[\beta_0-12\alpha(t)]\times I_{Pentamers}(q)+[\gamma_0-\alpha(t)]\times I_{RNA}(q) \quad (3)$$

where β_0 and γ_0 are the initial concentrations of the VP1 pentamers and RNA, respectively (there were no VLPs at time zero).

Indeed, the fit of the normalized basis spectra of pure reaction components (Figure S3) to the scattering data of Figure 3A are consistent with a two state reaction as describe by eq 3 (Figure S4). Furthermore, the observed isosbestic point is unlikely to form with more than two dominating states (reactants and product, as in eq 3).

From fitting the data to eq 3, we obtained the concentration of RNA-filled VLPs as a function of time (Figure 3B). Individual experiments were very consistent; the reaction time course represents data from 5 individual assembly reactions with measurements taken at different delays. At 30 ms, there is more than 0.15 μM capsid out of a theoretical maximum of 0.5 μM. The first 2–3 seconds of the reaction produces nearly 90% of the steady state VLP concentration. The concentration of VLP at 20 seconds was approximately 0.45 μM, with no significant variation detected at later times. Repeating the reaction with slightly lower reactant concentrations, in the flow-through setup, showed that even at the lower concentration and longer reaction times (up to 4 min), there was no significant increase in the concentration of the product (Figure S6). This finding suggests that 0.45 μM is close to the steady-state concentration of VLPs, under the conditions of our measurements.

Master Equation Modeling of Assembly using TR-SAXS data

SAXS data informed development of a model of VLP assembly. Initially, two alternatives were considered. In the first model, VLPs would form by binding of $VP1_5$ to 500 mer RNA (eq 4); intermediates would be partial capsids, expected to be present at low concentrations. [16] In the second alternative, 12 $VP1_5$ would form an amorphous complex with a 500 mer that would then anneal to a compact VLP (eq 5). [31,32] These are the simplified models:

$$12\,VP1_5+RNA \rightarrow VLP, \quad (4)$$

$$12\,VP1_5+RNA \rightarrow \text{amorphous complex} \rightarrow VLP. \quad (5)$$

The SAXS data indicate that assembly is very rapid with no measurable intermediate concentrations, effectively a two state reaction. The annealing step is thus either very fast or altogether absent. Therefore, subsequent rigorous assembly models were based on the assumption of stepwise association of pentamers to the RNA. Based on previous experience with such models, [16,33] we incorporated the possibility of a rate-limiting nucleation step, where the first n subunits associated with one another and with the RNA at a slower rate and/or weaker association energy.

$$nVP1_5+RNA \underset{k_{D_{nuc,j}}}{\overset{k_{nuc,j}}{\rightleftarrows}} nucleus_n\,(nucleation). \quad (6)$$

The nucleation step is followed by a series of (12 - n) elongation steps:

$$VP1_5{+}nucleus_n \underset{k_{D,j}}{\overset{k_{f,j}}{\rightleftarrows}} VP1_5{+}nucleus_{n+1} \underset{k_{D,j}}{\overset{k_{f,j}}{\rightleftarrows}} \ldots\ldots\ldots \underset{k_{D,12}}{\overset{k_{f,12}}{\rightleftarrows}} VLP \quad (elongation). \tag{7}$$

Nucleation begins with the first subunit binding to RNA with a rate of $k_{nuc,j}$ and a dissociation rate of $k_{D_{nuc}j}$. The index j indicates that the rate constant for association or dissociation of each pentamer will include terms for the degeneracy of assembly and disassembly and for the number of pentamer-pentamer interactions that form or brake during assembly or disassembly (see ref [34]). After the nucleating pentamer(s) bind, the subsequent (12-n) "elongation" reactions occur at association rates of $k_{f,j}$ and dissociation rates of $k_{D,j}$. The stability of the interactions appears in the dissociation term. For example, the last pentamer associates to a single site with a rate constant of $k_{f,12}$ whereas the corresponding dissociation could occur at any of twelve equivalent sites and will require simultaneous breaking of five inter-pentamer contacts (and VP1-RNA contact), each with an association energy of $\Delta G^0_{contact}$. (As the dissociation constant for reaction j, $K_{D,j}$, is equal to $k_{D,j}/k_{f,j}$, the resulting dissociation rate, $k_{D,12}$ is thus $12k_{f,12} \cdot \exp(-\Delta G^0_{contact}/RT)$, where R is the universal gas constant and T is temperature in Kelvin).

Models were tested for reactions with monomeric, dimeric, and trimeric nuclei. All three models fit the data extremely well (Figures 3B and S6). Further experiments with other initial concentrations might differentiate between different nuclei sizes. [21,35,36] Those experiments, however, are challenging because by increasing concentrations the kinetics becomes too rapid to follow by our TR-SAXS, whereas by lowering concentrations the signals become too weak to properly analyze. Residuals from comparison of observed assembly and calculated kinetic trajectories appear to be small and random and are similar for the three models (Figure S6). The root-mean-square deviation (RMSD) between observed and predicted values was about 7×10^{-9} M, which is ca. 1.5 % of the final VLP concentration. All three models generate undetectable concentrations of intermediates, consistent with the two-state behavior suggested by the isosbestic point and fitting of the TR-SAXS curves to essentially two basis spectra, associated with the product and the two reactants, using eq 3 (Figures 3A and S4). The last panel of Figure S6 shows that simulations predict that less than 4% of the total VP1 concentration will ever be present as intermediate and only at early times in the reaction.

Kinetic models were fit to our TR-SAXS data to allow extraction of rate and association constants (Table 1). To simplify comparisons, microscopic rate constants and association energies are provided in Table 1. (The microscopic constants are the underlying values stripped of statistical factors for reaction degeneracy, i.e., the fivefold symmetry of incoming pentamers and the number of available sites on a given intermediate.) including the reaction degeneracy ($-RT\ln(5^{11}/12)$), [16] the overall association energy of the capsid is thus about −95 kcal/mol (159 $k_B T$). The nucleation phase of assembly is characterized by a slow rate and strong association energy compared with the elongation phase. This process is contrary to classical polymerization reactions where nucleation is characterized by weak association energy compared with that of elongation. In our case, however, nucleation is dominated by the relatively slow and relatively strong pentamer-RNA interaction. Therefore, the delineation between the nucleation and elongation phases of assembly is kinetic. Simulations indicate that elongation may be as much as 150-fold faster than nucleation. Though elongation is very fast, with an average value of 6×10^9 M^{-1} s^{-1}, the per-contact association energy for elongation is very weak; only about −2.7 kcal/mol per contact, corresponding to 10 mM dissociation constant. Nevertheless, as each $VP1_5$ is pentavalent, the pseudo-critical concentration of assembly is proportional to $5/2 \cdot \Delta G^0_{contact}$,

corresponding to 10 μM; the added energy of nucleation brings the pseudo-critical $VP1_5$ concentration to between 0.6 and 2.1 μM, which compares well with the observed concentration of free pentamers of approximately 2 μM (Figures 1 & S1).

DISCUSSION

Using 500 mer RNA, we have shown that we can drive formation of *T*=1 VLPs from SV40 $VP1_5$. Using TR-SAXS, we show that the kinetics of RNA-driven SV40 VLP formation is very fast, yet can be described in terms of simple nucleated assembly followed by elongation steps (Figure 4). Similar models accurately describe assembly of empty capsids from many different viruses. [37] Application to experimental observation of nucleic acid-driven assembly has provided surprising results. A close examination of assembly parameters shows that the interactions of protein and nucleic acid is important for the regulation of assembly, and long range electrostatics are imperative for attracting reactants.

Surprisingly, the binding of the first pentamers to the 500 mer RNA molecule and protein-protein self-association on the RNA were astoundingly weak, about −6 kcal/mol (Table 1). Elongation energies, which are the pairwise interaction energies including contribution from nucleic acid, were even weaker, about −2.7 kcal/mol for all elongation steps (Table 1). In the assembly models, the association energy has contributions from protein-protein and protein-RNA interaction. Thus, in the monomeric nucleation model, where assembly is nucleated by the association of the first pentamer to the 500 mer, the nucleation center association energy only reflects binding of $VP1_5$ to RNA (other forms of nucleation include contributions from protein-protein interaction modulated by association rate). The estimated RNA - $VP1_5$ association energy of −6.48 kcal/mol (Table 1) corresponds to a dissociation constant of 15 μM. By comparison, the dissociation constant determined for binding of $VP1_5$, truncated for its C-terminal arms, to DNA was 2 – 7 nM [10], more than 3 orders of magnitude lower. These results indicate a thermodynamic barrier to binding of wt $VP1_5$ (with full C-termini) to RNA. Because the high affinity nucleic acid binding occurs in a C-terminus truncated protein [10,38] the VP1's C-terminal arm is likely to act as governor for nucleic acid binding and assembly. This is supported by a study on chaperone-assisted assembly, [38] which appears to require a C-terminus bound protein. Indeed, crystal structure of polyomavirus unassembled pentamers (truncated for the C-arm and part of the N-arm) shows that the conformation of the DNA binding domain (which is at the N-terminus) is altered during assembly, suggesting that in the unassembled pentamers the C-terminus occludes the nucleic acid binding domain. [39]

The mutual occlusion of both C and N-termini was proposed as a mechanism that prevents self-invasion of C-arms into their parent-pentamer, a process that would poison assembly. [39] We propose that the conformational change, releasing both termini, is triggered by pentamer binding to the nucleic acid. This binding is followed by pentamer sliding along the nucleic acid to an appropriate position, allowing the released C-termini to connect with neighboring pentamers (Figure 4). Analysis of virus assembly thermodynamics is in its infancy: To our knowledge, only HBV and phage MS2 have previously been shown to regulate their assembly using a conformationally assembly-inactive state. [40–42]

It is also worth iterating that we did not observe intermediates during SV40 VLP assembly. One expectation was that we would see rapid formation of an unstructured nucleoprotein complex that would anneal. [31,32] Such would be the case if binding to nucleic acid was fast but formation of protein-protein contacts relatively slow; we observed no evidence of an initial complex that matured into the *T*=1 conformation. Disordered intermediate complexes of RNA and pentamers consist of various conformations, shapes, and sizes. Each structure has a different scattering contribution to the signal. The sum of the contributions typically

results in a decaying curve rather than the observed oscillating signal (Figure 3A) that well fit a well-defined structural model (Figure S4). The observed spectra are well-described as a linear combination of reactants (RNA and $VP1_5$) and T=1 VLP normalized basis spectra. Furthermore, the absence of unstructured capsids indicates that there was no special barrier to self-association of subunits. Indeed, assembly was highly cooperative (Figures 1 and 3 and Figure S1), which indicates that protein interactions were attractive and facile. [43] Another expectation was that incorporation of the last few subunits would be very difficult. This expectation arose from simulations of assembly of empty capsids, where the last few subunits were kinetically impeded, probably by the decreasing target size, [44,45] or kinetically and thermodynamically impeded by partial blockage of the site due to capsid breathing. [46] Even if complete and nearly complete VLPs would be undistinguishable, accumulation of incomplete intermediates would contribute differently to the scattering signal than any linear combination of the basis spectra used in eq 3. Dissection, however, of the SAXS spectra in terms of RNA, $VP1_5$ and VLP was well-described by a single parameter fit (Figure S4 and eq 3), indicating that almost complete capsids, like other intermediates (or incomplete capsids), were not present at detectable concentrations.

Kinetics of RNA-induced $VP1_5$ assembly were very fast though 13 components (12 pentamers and an RNA molecule) participate in the reaction. In spite of the possibilities for intermediates and off-path complexes, only reactants and completed VLP were evident during the reaction. The two-state appearance is precisely the expectation for nucleated capsid assembly, where rare nuclei are rapidly consumed as soon as they appear. [16] The surprising point is that addition of the first nucleating pentamer/s to RNA was two orders of magnitude slower compared with subsequent elongation (Table 1). If we postulate that a conformational change is required to form the $VP1_5$-RNA interactions, the elongation reactions must be accelerated by direct interaction with the growing capsid, presumably by an induced fit mechanism.

The kinetic rate constants, for both nucleation and elongation, were stunningly fast. The elongation rates calculated from different models are lower-bound estimates of the actual association rates; the k_f values are microscopic rates that ignore degeneracy coefficients of up to 30 fold for the rate limiting steps. Unusually fast kinetics for protein-nucleic acid interactions, however, are not uncommon, facilitated by one dimensional diffusion of positively charged protein along negatively charged nucleic acid and by long-ranged electrostatic steering. [47] Note that under the experimental (physiological) conditions the Debye screening length is between 1 and 2 nm.

All three kinetic models (Figure 3B and Figure S6) have two common features: the nucleation step is much slower than subsequent elongation and, surprisingly, nucleation is much lower energy than elongation (Table 1). Thus, the limiting factor of VLP assembly is the kinetics of nucleation. Editing the data causes modest changes in the quantitation of energy and rate. A simpler model based on two rate constants and a single association energy did not fit the data; this suggests that the model with unique rate and association constants for nucleation and elongation steps represents the minimal chemically realistic model. Furthermore, the summed ΔG values from the curve fit (Figure 3), as modified by entropic statistical terms, are in agreement with the overall association energy. To derive more precise reaction constants will require a global comparison of a broad range of solution conditions to master equations with differing nucleation steps (as shown in this paper) and varying selections of possible intermediates. [33,48]

Calculations and coarse-grained dynamic simulation [45,49] estimated the role of nucleic acid length, and the ratio between the protein - nucleic acid and protein - protein interactions on the assembled structure and assembly mechanism. Those studies show that when the nucleic

acid is short (e.g. 500 mer, as in our study), T =1 particles are expected. [45] Nucleation and elongation assembly mechanism is expected for short RNA and when the protein - protein attraction energy is of the same order of magnitude as the protein-RNA attraction, consistent with our finding (Table 1). [45] Simulations [49] show that the capsid protein sticks to the RNA through electrostatic interactions and slides along the RNA chain toward the assembly site. This sliding process is considered as one-dimension diffusion and increases the rate of assembly. The ssRNA has been described by von Hippel and co-workers [47] to serve as an antenna, collecting the capsid proteins from the solution, and guiding them to the assembly site (Figure 4). [49]

Coarse grained simulations support the antenna hypothesis but particularly emphasize the role of the antenna in nucleating assembly. [45,50] These calculations predict that the RNA antenna effect will be attenuated as the nucleic acid is adsorbed by the addition of pentamers. The calculations, however, dramatically understate the situation observed in the TR-SAXS experiments. We observe that assembly is very fast even when the RNA is all but encapsidated. We offer a simple explanation that is general to many viruses: the exterior of the capsid is negatively charged, while the protein nucleic acid binding surface is positively charged, creating a huge dipole for the incoming subunit (Figures 4 and S7). Thus both exposed nucleic acid and the negatively charged incipient exterior of the growing capsid act together as an electrostatic attractant. [27] Though only a small gap may remain on the growing capsid, two-dimensional diffusion of the incoming subunit over the exterior surface is likely to be very fast. Postulating that the negatively charged capsid exterior, which grows during assembly, acts as an antenna leads to the distinct possibility that it will support progressively increased apparent rates of subunit addition.

CONCLUSIONS

We have shown that a short RNA molecule induces rapid assembly of 12 SV40 VP1 pentamers to form a T = 1 VLP. Our high-resolution synchrotron time-resolved solution small-angle X-ray scattering (TR-SAXS) data are consistent with a two state reaction; reactants (VP1 pentamers and RNA) and RNA-filled VLPs. Intermediate concentrations were immeasurably low. Assembly trajectories were well fit by models based on nucleated, stepwise assembly. Reaction parameters based on the models indicate that the nucleation phase was kinetically-limited [21] and that interpentamer association energies were very weak. In nature the interpentamer bonding of SV40 is stabilize by Ca^{2+} ions, 2 ions per monomer (10 per pentamer), that lock the C-arms in neighboring pentamers. [11] The kinetics of the reaction has interesting implications for assembly *in vivo*. Hypothetically, once assembly is initiated, speed and cooperativity will allow viruses to assemble with minimal interference from host defenses. The basis of the speed of assembly is likely to be the long-range electrostatic interactions afforded by the positive charge of the incoming subunit ($VP1_5$), attracted to the negative charge of the nucleic acid and the negative charge of the exterior of the growing capsid. As evidence of external negative charge, many viruses, including SV40, migrate to the anode during native agarose gel electrophoresis (Figure 1 and Figure S1). One can speculate that viruses use this charge to achieve the antenna effect in the crowded environs of the cell.

Supplementary Material

Refer to Web version on PubMed Central for supplementary material.

Acknowledgments

Funding Sources

US–Israel Binational Science Foundation (BSF) grant number 2005050 and NIH R01-AI077688.

We gratefully acknowledge use of the ID02 beamline at the ESRF synchrotron and thank J. Gummel, S. Callow and T. Naryanan for experimental help and useful discussions. We thank W. M. Gelbart for helpful discussions. Micrographs were recorded at the Indiana Molecular Biology Institute EM facility. Support for this project was provided by the Safra, Wolfson, and Rudin foundations (UR), the James Franck and Fritz Haber Minerva Centers (UR and DH), the Hebrew University Nanocenter (RA), the US–Israel Binational Science Foundation (BSF) grant number 2005050 (AO and AZ), and NIH R01-AI077688 (AZ).

ABBREVIATIONS

VLP	virus-like particles
SAXS	small-angle X-ray scattering
TR-SAXS	time-resolved SAXS
EMSA	electrophoretic mobility shift assay
TEM	transmission electron microscopy

References

1. Young M, Willits D, Uchida M, Douglas T. Annu Rev Phytopathol. 2008; 46:361. [PubMed: 18473700]
2. Kang S, Uchida M, O'Neil A, Li R, Prevelige PE, Douglas T. Biomacromolecules. 2010; 11:2804. [PubMed: 20839852]
3. Aniagyei SE, Dufort C, Kao CC, Dragnea B. J Mater Chem. 2008; 18:3763. [PubMed: 19809586]
4. Dragnea B. Nat Mater. 2008; 7:102. [PubMed: 18219330]
5. Kimchi-Sarfaty C, Ben-Nun-Shaul O, Rund D, Oppenheim A, Gottesman MM. Hum Gene Ther. 2002; 13:299. [PubMed: 11812285]
6. Arad U, Zeira E, El-Latif MA, Mukherjee S, Mitchell L, Pappo O, Galun E, Oppenheim A. Human gene therapy. 2005; 16:361. [PubMed: 15812231]
7. Li W, Asokan A, Wu Z, Van Dyke T, DiPrimio N, Johnson JS, Govindaswamy L, Agbandje-McKenna M, Leichtle S, Redmond DE Jr, McCown TJ, Petermann KB, Sharpless NE, Samulski RJ. Mol Ther. 2008; 16:1252. [PubMed: 18500254]
8. Griffith J, Dieckmann M, Berg P. J Virol. 1975; 15:167. [PubMed: 163341]
9. Varshavsky AJ, Bakayev VV, Chumackov PM, Georgiev GP. Nucleic Acids Research. 1976; 3:2101. [PubMed: 184438]
10. Li PP, Nakanishi A, Shum D, Sun PC, Salazar AM, Fernandez CF, Chan SW, Kasamatsu H. J Virol. 2001; 75:7321. [PubMed: 11462004]
11. Stehle T, Gamblin SJ, Yan Y, Harrison SC. Structure. 1996; 4:165. [PubMed: 8805523]
12. Li PP, Nakanishi A, Clark SW, Kasamatsu H. Proc Nat'l Acad Sci USA. 2002; 99:1353.
13. Liddington RC, Yan Y, Moulai J, Sahli R, Benjamin TL, Harrison SC. Nature. 1991; 354:278. [PubMed: 1659663]
14. Sandalon Z, Oppenheim A. Virology. 1997; 237:414. [PubMed: 9356352]
15. Mukherjee S, Abd-El-Latif M, Bronstein M, Ben-nun-Shaul O, Kler S, Oppenheim A. PLoS One. 2007; 2:e765. [PubMed: 17712413]
16. Katen SP, Zlotnick A. Methods in Enz. 2009; 455:395.
17. Rapaport DC. Phys Rev Lett. 2008; 101:186101. [PubMed: 18999841]
18. Zlotnick A. J Mol Biol. 2007; 366:14. [PubMed: 17157314]
19. Prevelige PE, Thomas D, King J. Biophys J. 1993; 64:824. [PubMed: 8471727]
20. Zlotnick A, Aldrich R, Johnson JM, Ceres P, Young MJ. Virology. 2000; 277:450. [PubMed: 11080492]
21. Zlotnick A, Johnson JM, Wingfield PW, Stahl SJ, Endres D. Biochemistry. 1999; 38:14644. [PubMed: 10545189]

22. Porterfield JZ, Dhason MS, Loeb DD, Nassal M, Stray SJ, Zlotnick A. J Virol. 2010; 84:7174. [PubMed: 20427522]
23. Johnson JM, Tang J, Nyame Y, Willits D, Young MJ, Zlotnick A. Nano Lett. 2005; 5:765. [PubMed: 15826125]
24. Johnson JM, Willits D, Young MJ, Zlotnick A. J Mol Biol. 2004; 335:455. [PubMed: 14672655]
25. Mukherjee S, Kler S, Oppenheim A, Zlotnick A. Virology. 2010
26. Szekely, Ginsburg A, Ben-Nun T, Raviv U. Langmuir. 2010; 26:13110. [PubMed: 20695550]
27. Szekely O, Steiner A, Szekely P, Amit E, Asor R, Tamburu C, Raviv U. Langmuir. 2011; 27:7419. [PubMed: 21598965]
28. Nadler M, Steiner A, Dvir T, Szekely O, Szekely P, Ginsburg A, Asor R, Resh R, Tamburu C, Peres M, Raviv U. Soft Matter. 2011; 7:1512.
29. Hammersley AP, Svensson SO, Hanfland M, Fitch AN, Hausermann D. High Pressure Res. 1996; 14:235.
30. Ben-Nun T, Ginsburg A, Szekely P, Raviv U. Journal of Applied Crystallography. 2010; 43:1522.
31. McPherson A. Bioessays. 2005; 27:447. [PubMed: 15770675]
32. Hagan MF. J Chem Phys. 2009; 130:114902. [PubMed: 19317561]
33. Moisant P, Neeman H, Zlotnick A. Biophysical Journal. 2010; 99:1350. [PubMed: 20816046]
34. Zlotnick A. J Mol Biol. 1994; 241:59. [PubMed: 8051707]
35. Endres D, Zlotnick A. Biophys J. 2002; 83:1217. [PubMed: 12124301]
36. Hagan MF, Elrad OM. Biophys J. 2010; 98:1065. [PubMed: 20303864]
37. Zlotnick A, Mukhopadhyay S. Trends Microbiol. 2011; 19:14. [PubMed: 21163649]
38. Chromy LR, Pipas JM, Garcea RL. Proc Natl Acad Sci U S A. 2003; 100:10477. [PubMed: 12928495]
39. Stehle T, Harrison SC. EMBO J. 1997; 16:5139. [PubMed: 9305654]
40. Ceres P, Zlotnick A. Biochemistry. 2002; 41:11525. [PubMed: 12269796]
41. Packianathan C, Katen SP, Dann CE 3rd, Zlotnick A. J Virol. 2010; 84:1607. [PubMed: 19939922]
42. Stockley PG, Rolfsson O, Thompson GS, Basnak G, Francese S, Stonehouse NJ, Homans SW, Ashcroft AE. J Mol Biol. 2007; 369:541. [PubMed: 17434527]
43. McGhee JD, von Hippel PH. J Mol Biol. 1974; 86:469. [PubMed: 4416620]
44. Rapaport DC. Phys Rev E Stat Nonlin Soft Matter Phys. 2004; 70:051905. [PubMed: 15600654]
45. Elrad OM, Hagan MF. Phys Biol. 2010; 7:045003. [PubMed: 21149971]
46. Nguyen HD, Reddy VS, Brooks CL 3rd. Nano Lett. 2007; 7:338. [PubMed: 17297998]
47. von Hippel PH, Berg OG. J Biol Chem. 1989; 264:675. [PubMed: 2642903]
48. Endres D, Miyahara M, Moisant P, Zlotnick A. Protein Science. 2005; 14:1518. [PubMed: 15930000]
49. Hu T, Shklovskii BI. Phys Rev E Stat Nonlin Soft Matter Phys. 2007; 75:051901. [PubMed: 17677092]
50. Kivenson A, Hagan MF. Biophysical journal. 2010; 99:619. [PubMed: 20643082]

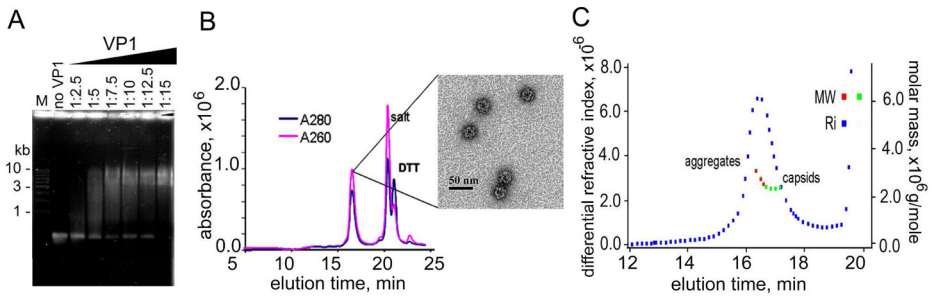

Figure 1.

Assembly of VP15 with 524 nt RNA molecules, stoichiometry and mass of 22 nm capsids. A. Titration of 524 nt RNAs with VP1 pentamers. Electrophoretic mobility shift assay (EMSA) was analyzed by 0.6% agarose gels. B. Size exclusion chromatography (SEC) of capsids assembled on 524 nt RNA. The A260/A280 absorbance ratio corresponds to 12 VP1 pentamers per one RNA molecule. Inset: TEM image of the fraction collected from the absorbance peak, showing only 22 nm capsids. C. Multi-Angle Laser Light Scattering (MALLS) of the capsids assembled on 524 nt RNA. The molecular weight of the capsids is 2.6 MDa, as expected for T=1 capsid.

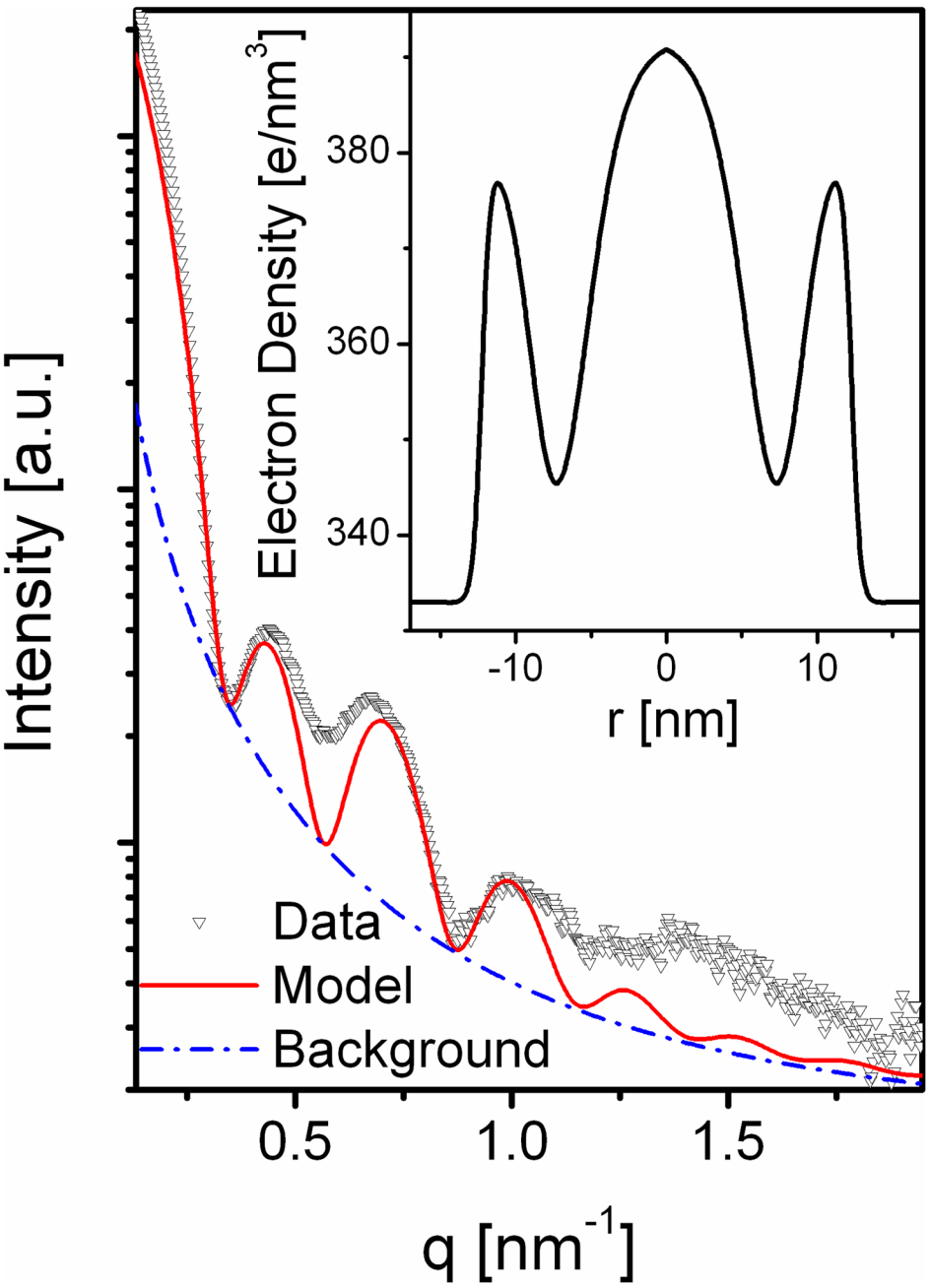

Figure 2.

Radially integrated solution small X-ray scattering (SAXS) intensity from steady-state (*T*=1) 500mer RNA VLPs (open symbols). The solid curve is the best fitted form-factor model of multiple spherical shells with a smoothly varying radial electron density profiles, represented by hyperbolic tangent functions (eq 1) and shown at the inset. The broken curve shows the assumed power-law background given by $0.261q^{2.061} + 0.142$. The best fitted parameters for eq 1 are: $\Delta\rho_1 = 58.9$ e/nm^3, $\Delta\rho_2 = -18.0$ e/nm^3, $\Delta\rho_3 = 48.5$ e/nm^3 (the electron density of the buffer is assume to be similar to that of water: 333 e/nm^3), $R_1 = 5.7$ nm, $R_2 = 3.0$ nm, $R_3 = 3.5$ nm, $s_1 = 0.4$, $s_2 = 0.5$ and $s_3 = 1.7$.

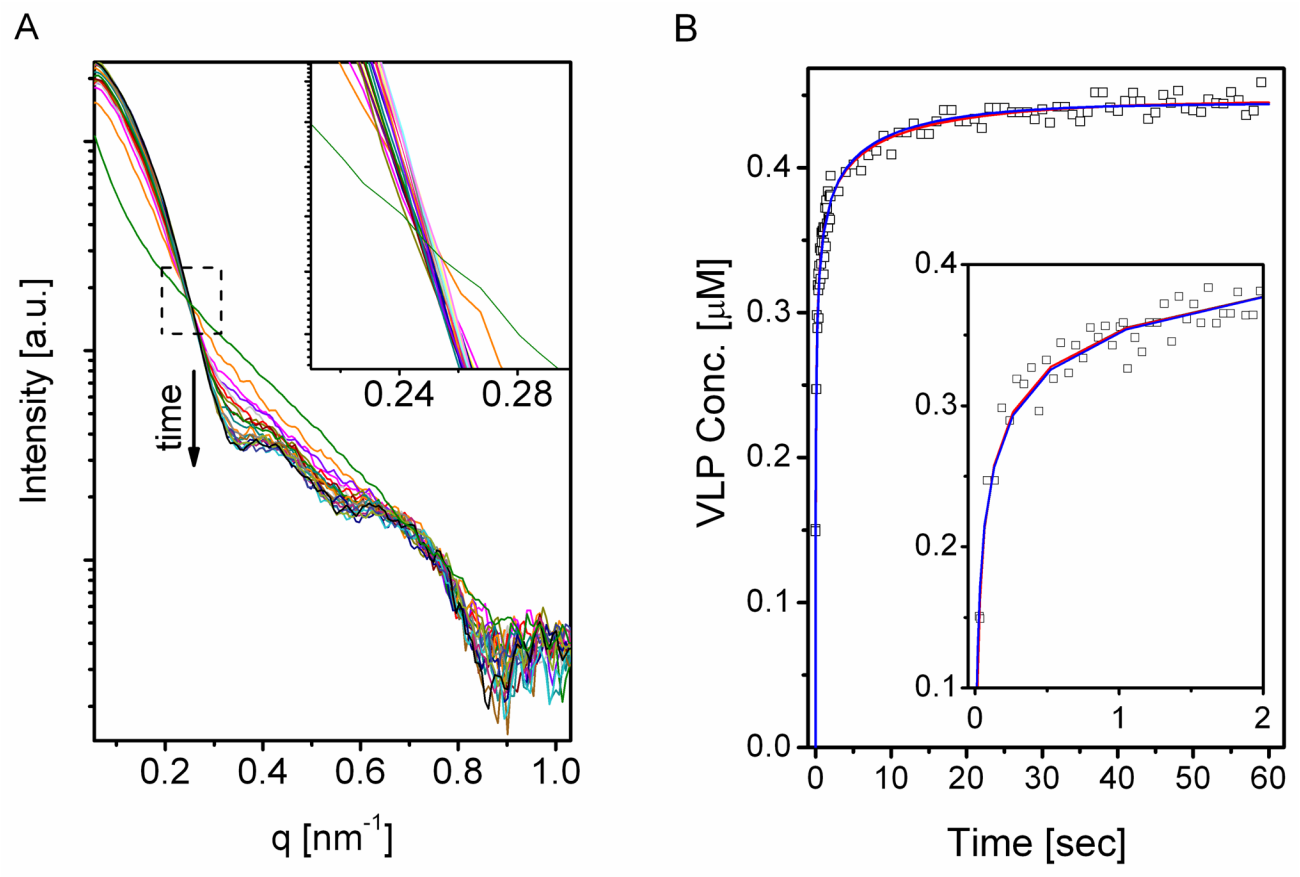

Figure 3.

TR-SAXS data and kinetic analysis. **A.** Radially integrated TR-SAXS measurements during the assembly process of the T=1 VLPs. The time, *t*, elapsed after mixing 0.5 μM 500 mer RNA and 7.5 μM VP1 pentamers is between 35 ms (Orange curve) and 59 sec (Black curve). The signal that corresponds to $t = 0$ (Green curve) is represented by the sum of the measured scattering intensities of a solution of 7.5 μM VP1 pentamers and a solution of 0.5 μM 524 nt ssRNA. The inset shows the isosbestic point at q ~ 0.25 nm^{-1} on an expanded scale. For clarity, the figure shows only selected time points. **B.** Concentration of the formed T=1 RNA VLPs as a function of time, t, fit to predicted assembly kinetics (eqs 6 and 7). The inset shows the first 2 sec on an expanded scale. The concentrations were obtained by fitting the scattering curves shown in **A** to eq 3 (Figure S4). The reaction kinetics were modeled assuming the RNA initially nucleated either with a VP1 pentamer (blue curve), a dimer of pentamers (red curve), or a trimer of pentamers (black solid curve; not seen due to overlap with the red curve). Separate curve fits, residuals, and the negligible fraction of intermediate structures in each model are shown in Figure S6.

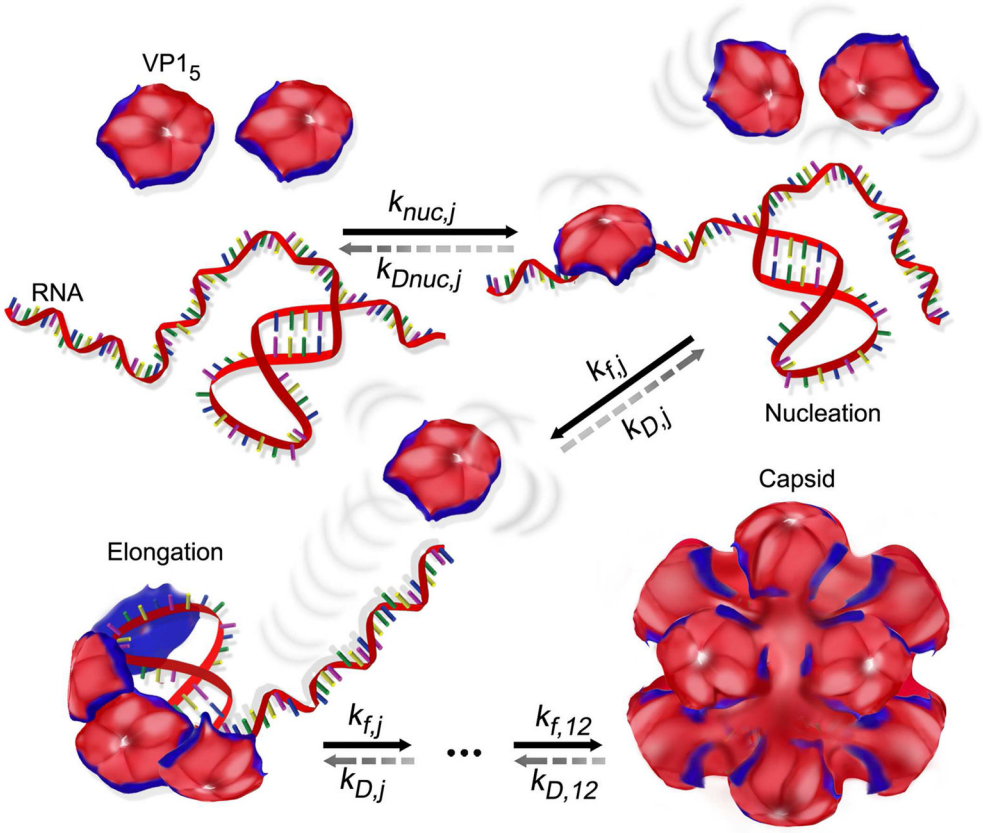

Figure 4.

The nucleoprotein antenna model of assembly. The cartoon depicts assembly of SV40 VP1 pentamers on an RNA substrate. The RNA and the external surface of the pentamers are negatively charged, as indicated by the red color. The inner surface of the pentamer has a positively charged nucleic acid-binding surface, shown in blue. Thus, each pentamer is intrinsically dipolar. Free pentamers are attracted to the negatively charged RNA via their positively charged inner surface. Nucleation is shown here as attachment of a single pentamer to the RNA. The partly packaged RNA and the exterior of the growing capsid are both negatively charged and can thus function together as an antenna to attract additional capsomers. Elongation is facilitated by electrostatic attraction of pentamers and their diffusion (or sliding), along RNA and the exterior of the incomplete capsid, to the next assembly site until assembly is completed. Thus the assembly rate continues to be very rapid throughout the assembly reaction although the RNA is progressively packaged.

Table 1

Kinetic constants. Constants from kinetics curve fits to the concentration of the formed *T*=1 virus-like particles as a function of time. Simulations are based on reaction of 7.5 μM $VP1_5$ with 0.5 μM 500mer RNA. The consensus is a simple average.

	Size of pentamer nucleus			
Constant	**Monomeric**	**Dimeric**	**Trimeric**	**Consensus**
k_{nuc} (M^{-1} s^{-1})	9.3×10^{7}	2.2×10^{7}	0.9×10^{7}	**4×10^{7}**
Δ G_{nuc} (kcal/mol)	−6.48	−4.74	−6.03	**− (5.8±0.9)**
k_f (M^{-1} s^{-1})	1.81×10^{10}	7.32×10^{8}	4.3×10^{8}	**6×10^{9}**
Δ G_{elong} (kcal/mol)	−2.58	−2.96	−2.54	**− (2.7±0.2)**
k_f/k_{nuc}	201	33	48	**90**